actuators

Article

Conceptual Approach to Permanent Magnet Synchronous Motor Turn-to-Turn Short Circuit and Uniform Demagnetization Fault Diagnosis

Yinquan Yu [1,2], Chun Yuan [1,2], Dequan Zeng [1,2], Giuseppe Carbone [1,3,*], Yiming Hu [1,2] and Jinwen Yang [1,2]

[1] School of Mechatronics and Vehicle Engineering, East China Jiaotong University, Nanchang 330013, China; yu_yinquan@ecjtu.edu.cn (Y.Y.); 2022038080200022@ejctu.edu.cn (C.Y.); 3340@ejctu.edu.cn (D.Z.); huyiming139@hotmail.com (Y.H.); 8652@ejcut.edu.cn (J.Y.)
[2] Key Laboratory of Conveyance and Equipment of Ministry of Education, Institute of Precision Machining and Intelligent Equipment Manufacturing, East China Jiaotong University, Nanchang 330013, China
[3] Department of Mechanical, Energy, and Management Engineering, University of Calabria, 87036 Rende, Italy
* Correspondence: giuseppe.carbone@unical.it

Abstract: Permanent magnet synchronous motors (PMSMs) play a crucial role in industrial production, and in response to the problem of PMSM turn-to-turn short-circuit and demagnetization faults affecting production safety, this paper proposes a PMSM turn-to-turn short-circuit and demagnetization fault diagnostic method based on a convolutional neural network and bidirectional long and short-term memory neural network (CNN-BiLSTM). Firstly, analyzing the PMSM turn-to-turn short-circuit and demagnetization faults, one takes the PMSM stator current as the fault signal and optimizes the variational modal decomposition (VMD) by using the Gray Wolf Optimization (GWO) algorithm in order to achieve efficient noise reduction processing of the stator current signal and improve the fault feature content in the stator current signal. Finally, the fault diagnostics are classified by using the CNN-BiLSTM, which collects advanced optimization algorithms and deep learning networks. The effectiveness of the method is verified by simulation experiment results. This scheme has high practical value and broad application prospects in the field of PMSM turn-to-turn short circuit and demagnetization fault diagnosis.

Keywords: permanent magnet synchronous motor; turn-to-turn short circuit; demagnetization; fault diagnosis

Citation: Yu, Y.; Yuan, C.; Zeng, D.; Carbone, G.; Hu, Y.; Yang, J. Conceptual Approach to Permanent Magnet Synchronous Motor Turn-to-Turn Short Circuit and Uniform Demagnetization Fault Diagnosis. *Actuators* **2024**, *13*, 511. https://doi.org/10.3390/act13120511

Academic Editor: Giorgio Olmi

Received: 23 October 2024
Revised: 23 November 2024
Accepted: 7 December 2024
Published: 9 December 2024

1. Introduction

With the advantages of simple structure, high torque density, strong overload capacity, and wide speed regulation range, PMSMs are widely used in industrial automation, new energy vehicles, aerospace, wind power generation, and other industries [1–5]. As PMSMs are in harsh and complex working environments for a long time, this can lead to failures [6]. Turn-to-turn short-circuit faults occur when the insulating windings are damaged, when the turn-to-turn insulation is subjected to transient overvoltage during motor startup, or when the temperature of the windings is too high [7]. Demagnetization faults can also occur when the permanent magnets are subjected to high temperatures, strong external magnetic fields, and high currents [8]. Failure to detect these two types of faults in a timely manner can deepen the severity of the fault and lead to motor burnout, resulting in economic losses and safety hazards. Currently, there are main methods based on mathematical model analysis, fault signal analysis, and machine learning for PMSM turn-to-turn short-circuit faults and demagnetization faults.

Refs. [9,10] established a turn-to-turn short circuit mathematical model to analyze the correlation between signals such as phase currents, zero sequence voltage signals, and the degree of faults for fault diagnosis. Bifeng [11] et al. established a stator and rotor dual coordinate system for PMSM, analyzed the air gap variation of the motor, and established an unbalanced magnetic pulling (UMP) model under uniform demagnetization and eccentricity faults. They verified the accuracy of the changed mathematical model by means of Maxwell and MATLAB calculations and mutually verified the accuracy of the modified mathematical model. The diagnostic method based on mathematical model analysis has the advantages of high diagnostic accuracy and reliability, but the modeling complexity is high, and the computational volume is large and has other difficulties.

Refs. [12–14] directly analyzed data such as stator current, vibration signals, and response current amplitude in the time and frequency domains to determine the degree of fault, and Hyeyun Jeong [15] et al. found that inter-turn short-circuit faults resulted in a decrease in the β-angle by comparing the difference between the magnitude of the currents and the angle of the faulty and normal motors under the same load torque, and they utilized this correlation to diagnose the fault. Yun Zhang [16] et al. combined the diagnostic methods of mathematical modeling and signal analysis to determine the fault type by detecting the difference change between normal and faulty motors and then used the difference between the dq-axis predicted currents and the dq-axis feedback currents for different fault models to identify the fault phases to complete the turn-to-turn short-circuit diagnostics. Jun Hang [17] et al. used the difference in amplitude between stator currents of the absolute value to perform turn-to-turn short circuit fault diagnosis. Refs. [18–20] performed frequency domain analysis of the fault signal to obtain the correlation between a specific number of harmonics and the fault for fault diagnosis. Fang J. [21] et al. removed the noise and harmonic components in the zero-sequence voltage component by discrete wavelet transform, and used fast Fourier analysis of the optimized zero-sequence voltage signal for the turn-to-turn short-circuit fault diagnosis. Hang J. [22] et al. proposed a model prediction and control method for turn-to-turn short-circuit fault diagnosis based on the model predictive control for turn-to-turn short-circuit fault diagnosis by using wavelet transform to extract the demagnetization fault related eigenvalues from the cost function present in the model predictive control system and calculating the related eigenvectors for turn-to-turn diagnosis with wavelet transform coefficients. PMSM fault diagnosis based on signal analysis has the advantages of wide applicability and real-time and non-invasive diagnosis, but the selected fault signal is susceptible to electromagnetic interference and the influence of noise leading to misdiagnosis, and it requires professional knowledge and experience to process and analyze the signal.

Zhichao Chen [23] et al. used phase voltage, rotor electrical angle and rotor speed as inputs to the neural network and phase current as outputs of the neural network and compared the predicted current of the neural network's outputs with the actual measured currents for turn-to-turn short-circuit diagnostics. Hojin Lee [24] et al. chose the positive-sequence voltages and currents to negative-sequence voltages and currents as inputs of fault signals to a self-attentive severity estimation network to quantify the turn-to-turn short circuit and demagnetization fault severity. Refs. [25,26] et al. analyzed the stator current signal in the frequency domain to get the fault characteristics and used a support vector machine as well as a convolutional neural network for fault diagnosis. Haibin Huangfu [27] et al. performed the turn-to-turn short-circuit fault diagnosis based on the VGG16 deep convolutional neural network with migration learning, which used the three-phase stator current signal as the input for the fault diagnosis, and the grid search and cross-validation method were used to fine-tune the hyper-parameters in the network model. Siyuan Liang [28] et al. used stator current and vibration signals as fault diagnostic inputs and extracted the first and second sparse coefficients of the two signals using a sparse representation method, and they utilized a support vector machine to classify the turn-to-turn faults. Yuanjiang Li [29] et al. used a conditional generation adversarial network and an optimized sparse autoencoder to diagnose turn-to-turn faults based on a conditional generation adversarial network and optimized the sparse autoencoder network and optimized sparse autoencoder to complete the PMSM turn-to-turn short-circuit fault diagnosis, using a conditional generation adversarial network to increase the fault sample size. The machine learning-based PMSM fault diagnosis method has the advantages of high accuracy and reliability and can also adapt to complex working conditions and multi-fault diagnosis, and it has high automation and intelligence measurement.

Based on the above research, this paper combines the optimization algorithm and deep learning network, uses the optimized VMD to perform noise reduction on the original data, and then combines CNN-BiLSTM for fault diagnosis, which further improves the accuracy as well as robustness of the fault diagnosis of PMSM.

The rest of the paper is organized as follows: Section 2 presents the mathematical analysis of turn-to-turn short circuit faults and demagnetization faults of permanent magnet synchronous motors. Section 3 describes the optimized noise reduction method and the structure of the diagnostic network model. Section 4 performs diagnostic validation of the proposed method and compares it with other diagnostic methods. Section 5 summarizes the work of this paper.

2. Failure Analysis

2.1. Turn-to-Turn Short Circuit

Permanent magnet synchronous motor same-phase short-circuit caused by the winding insulation failure is called turn-to-turn short-circuit fault, and the permanent magnet synchronous motor is one of the most common electrical faults. Figure 1 illustrates the assumption that the permanent magnet synchronous motor A-phase turn-to-turn short-circuit faults occur after the simplification of the physical model. The figure uses R_a; R_b; R_c for the three-phase stator winding resistance, L_a; L_b; L_c for the three-phase stator winding inductance, and e_a; e_b; e_c for the three-phase winding induced electromotive force. When a turn-to-turn short-circuit fault occurs, the resistance and inductance of the fault-phase stator winding is divided into the normal part of the fault part of the R_{a1} and l_{a1}, e_{a2} is used for the resistance of the normal part of the resistance, as well as the inductance and the induction potential, R_{a2} and L_{a2}. e_{a2} is used for the normal part of the resistance and inductance and induction potential, and R_{a2} and L_{a2},e_{a2} are the resistance as well as inductance and induced electromotive force of the faulty part, and they satisfy $R_a = R_{a1} + R_{a2}$, $L_a = L_{a1} + L_{a2}$, $e_a = e_{a1} + e_{a2}$. Mutual inductance $\mathrm{M_{a1a2}}$ is generated between $\mathrm{L_{a1}}$ and $\mathrm{L_{a2}}$, and respectively, mutual inductance M_{a1b}; M_{a1c}; M_{a2b}; M_{a2c} is generated between B and C phases. Mutual inductance M_{bc}, i_a; i_b; i_c are the three-phase currents, while u_a; u_b; u_c are the three-phase voltages, R_f is the short-circuit resistance, and i_f is the short-circuit currents.

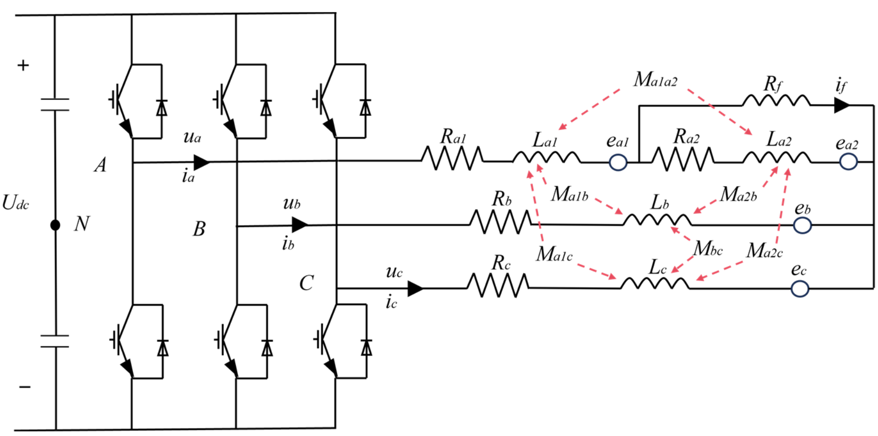

Figure 1. Physical modeling of turn-to-turn short circuits.

The ratio of the number of short-circuited turns to the total number of turns in phase A is called the short-circuited turns ratio defined as η, as shown in Equation (1).

$$\eta = \frac{n}{N} \tag{1}$$

where n is the number of short-circuit turns and N is the total number of turns in phase A.

The voltage equation after the occurrence of a turn-to-turn short circuit fault is given in Equation (2).

$$U_{f,abc} = R_{f,abc} I_{f,abc} + L_{sf} \frac{d}{dt} I_{f,abc} + \frac{d}{dt} \Psi_{sf} + U_0 \tag{2}$$

included among these

$$\begin{cases} U_{f,abc} = \begin{bmatrix} u_a & u_b & u_c & 0 \end{bmatrix}^{\mathrm{T}} \\ R_{f,abc} = \begin{bmatrix} R_s & 0 & 0 & \eta R_s \\ 0 & R_s & 0 & 0 \\ 0 & 0 & R_s & 0 \\ \eta R_s & 0 & 0 & \eta R_s + R_f \end{bmatrix} \\ I_{f,abc} = \begin{bmatrix} i_a & i_b & i_c & i_f \end{bmatrix}^{\mathrm{T}} \\ L_{sf} = \begin{bmatrix} L_a & M_{ab} & M_{ac} & \eta L_a \\ M_{ab} & L_b & M_{bc} & \eta M_{ba} \\ M_{ca} & M_{cb} & L_c & \eta M_{ca} \\ \eta L_a & \eta M_{ab} & \eta M_{ac} & \eta^2 L_a \end{bmatrix} \\ \Psi_{sf} = \begin{bmatrix} \Psi_{PM,a} & \Psi_{PM,b} & \Psi_{PM,c} & \Psi_{PM,f} \end{bmatrix}^{\mathrm{T}} \\ U_0 = \begin{bmatrix} u_0 & u_0 & u_0 & 0 \end{bmatrix}^{\mathrm{T}} \end{cases} \tag{3}$$

where $U_{f,abc}$ is the stator voltage matrix, $R_{f,abc}$ is the stator resistance matrix, $I_{f,abc}$ is the stator current matrix, L_{sf} is the stator inductance matrix, U_0 is the neutral voltage, and R_s is the stator resistance and is equal to the three-phase stator winding.

From Equation (3), the short-circuit current is given as Equation (4).

$$i_f = \frac{\eta(u_a - u_0)}{\eta(1-\eta)R_s + R_f} \tag{4}$$

where the neutral voltage u_0 is small relative to the stator voltage u_{a} and can be omitted. It can be simplified as Equation (5).

$$i_f \approx \frac{\eta u_a}{\eta(1-\eta)R_s + R_f} \tag{5}$$

It can be seen that when the turn-to-turn short-circuit fault occurs in phase A, the short-circuit turns ratio will affect the fault current and thus the phase A stator current, resulting in a three-phase current imbalance, and the turn-to-turn short-circuit fault will cause peak current fluctuations between the phase and the phase.

2.2. Uniform Demagnetization Failure Analysis

The permanent magnet synchronous motor in the three-phase stator winding magnetic chain equation can be expressed as Equation (6).

$$\begin{bmatrix} \lambda_{\mathrm{PMa}}(\theta, i) \\ \lambda_{\mathrm{PM_b}}(\theta, i) \\ \lambda_{\mathrm{PM_c}}(\theta, i) \end{bmatrix} = \begin{bmatrix} L_{\mathrm{aa}}(\theta) & M_{\mathrm{ab}}(\theta) & M_{\mathrm{ac}}(\theta) \\ M_{\mathrm{ba}}(\theta) & L_{\mathrm{bb}}(\theta) & M_{\mathrm{bc}}(\theta) \\ M_{\mathrm{ac}}(\theta) & M_{\mathrm{cb}}(\theta) & L_{\mathrm{cc}}(\theta) \end{bmatrix} \begin{bmatrix} i_{\mathrm{a}} \\ i_{\mathrm{b}} \\ i_c \end{bmatrix} + \begin{bmatrix} \lambda_{\mathrm{fa}} \\ \lambda_{\mathrm{fb}} \\ \lambda_{\mathrm{fc}} \end{bmatrix} \tag{6}$$

where L_{aa}, L_{bb}, L_{cc} are the self-inductance of the three-phase winding, M_{aa}, M_{ab}, M_{ac} are the mutual inductance of the three-phase winding, and λ_{fa}, λ_{fb}, λ_{fc} are the magnetic chains generated by the permanent magnet in the three-wire winding. It can be seen that when the permanent magnets are uniformly demagnetized, the internal magnetic field of the motor is still maintained to a certain degree of proportionality, but the parameters of the magnetic chains of the permanent magnets will be reduced. The strength of the magnetic field generated by the permanent magnet is weakened, resulting in a decrease in the synthesized magnetic kinetic potential inside the motor.

3. Proposed Method

3.1. Variational Modal Decomposition

The VMD algorithm is a non-recursive modal decomposition algorithm based on an adaptive filter, which can simultaneously estimate the modes with different center frequencies, thus avoiding the accumulation of errors in the envelope estimation and effectively solving the problems of endpoint effect and mode aliasing, which in turn improves the accuracy and stability of the modal decomposition, which can be denoised for the collected stator current signal of permanent magnet synchronous motor. The constrained variational modal decomposition model is shown as Equation (7):

$$\min_{\{\mu_k\}\cdot\{\omega_k\}} \left\{ \sum_k \left\| \partial_t \left[\left(\delta(t) + \frac{j}{\pi t} \right)^* \mu_k(t) \right] e^{-j\omega_k t} \right\|_2^2 \right\} \tag{7}$$

where $\mu_k = \{\mu_1,\ \mu_2, \ldots \mu_k\}$ is the K modal components obtained from decomposition; $\omega_k = \{\omega_1,\ \omega_2, \ldots,\ \omega_k\}$ is the frequency center of each single component; * is the convolution symbol; f_{signal} is the original signal; and t is time.

Introducing a quadratic penalty factor α and a Lagrange factor λ transforms the constrained variational problem into an unconstrained variational problem as in Equation (8).

$$\begin{gathered} L(\{\mu_k\}, \{\omega_k\}, \lambda) := \\ \alpha \sum_k \left\| \partial_i \left[\left(\delta(t) + \frac{j}{\pi t} \right)^* \mu_k(t) \right] e^{-j\omega_i t} \right\|_2^2 + \\ \left\| f(t) - \sum_k \mu_k(t) \right\|_2^2 + \left\langle \lambda(t), f(t) - \sum_k \mu_k(t) \right\rangle \end{gathered} \tag{8}$$

The alternating direction multiplier method is used to update μ_k and ω_k alternately to search for the saddle points of the augmented Lagrangian expression, and the final expressions of the IMF components and center frequencies are obtained as in Equations (9) and (10).

$$\hat{u}_k^{n+1}(\omega) = \frac{\hat{f}(\omega) - \sum_{i \neq k} \hat{u}_i(\omega) + \frac{\hat{\lambda}(\omega)}{2}}{1 + 2\alpha(\omega - \omega_k)^2} \tag{9}$$

$$\omega_k^{n+1} = \frac{\int_0^\infty \omega |\hat{u}_k(\omega)|^2 d\omega}{\int_0^\infty |\hat{u}_k(\omega)|^2 d\omega} \tag{10}$$

3.2. Gray Wolf Optimization

There are S individual gray wolves in the entire gray wolf population, and the location of the ith gray wolf is labeled $\mathrm{Xi} = \left\{ x_i^1, x_i^2, \ldots, x_i^d \right\}$. The optimal solution in the population is α, the second-best solution is β, the third-best solution is δ, and the remaining solution is ω. The position update is shown in Equation (11).

$$X(d+1) = X_{\text{target}}(d) - A \cdot \left| C \cdot X_{\text{target}}(d) - X(d) \right| \tag{11}$$

where d is the current iteration number, $X(d)$ and $X(d + 1)$ are the positions before and after the gray wolf moves, $X_{\text{target}}(d)$ is the target prey position, and A and C are the coefficient vectors. In this paper, we use GWO to optimize the number of decomposition layers as well as the penalty factor in the VMD to ensure that the VMD achieves the best decomposition effect.

3.3. One-Dimensional Convolutional Neural Network

The convolutional neural network mainly consists of an input layer, convolutional layer, activation layer, pooling layer, fully connected layer, and output layer. The convolutional kernel of the convolutional neural network is shared over the entire input to reduce the number of parameters of the model and reduce the model complexity. The one-dimensional convolutional neural network used in this paper is specialized for processing one-dimensional data.

3.4. BiLSTM

The structure of the long- and short-term memory neural network is shown in Figure 2, and the equations governing the amount of internal information are represented by Equations (12)–(17).

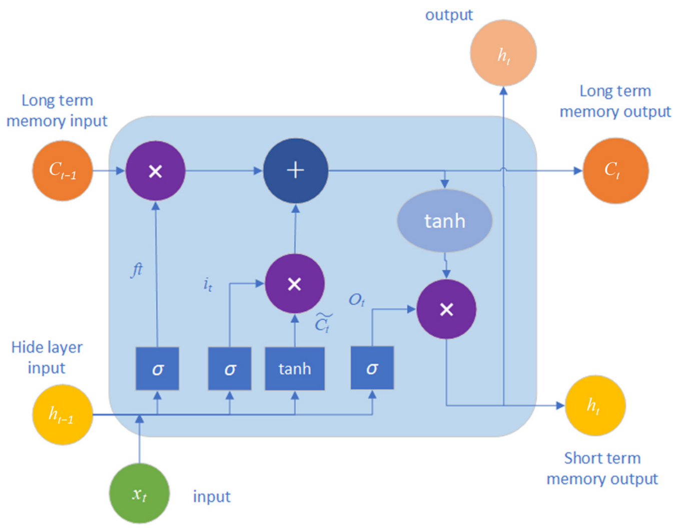

Figure 2. Long- and short-term memory neural network structure.

$$i_t = \sigma(x_t w_{xi} + h_{t-1} w_{hi} + b_i) \tag{12}$$

$$f_t = \sigma\left(x_t w_{xf} + h_{t-1} w_{hf} + b_f\right) \tag{13}$$

$$o_t = \sigma(x_t w_{xo} + h_{t-1} w_{ho} + b_o) \tag{14}$$

$$\tilde{c}_t = \tanh(x_t w_{xc} + h_{t-1} w_{hc} + b_c) \tag{15}$$

$$c_t = f_t \cdot c_{t-1} + i_t \cdot \tilde{c}_t \tag{16}$$

$$h_t = o_t \cdot \tanh(c_t) \tag{17}$$

where f_t is the output signal of the forgetting gate, indicating the proportion of forgetting of the memory cell C; i_t is the output signal of the output gate, indicating the proportion of the current input information to the memory cell; and O_t is the output signal of the output gate, indicating the proportion of the information output of the memory cell to the current state s.

The bi-directional long- and short-term memory neural network consists of a forward long- and short-term memory neural network and a backward long- and short-term memory neural network, where the forward direction is processed from the beginning to the end of the sequence, and the backward direction is processed from the end to the beginning of the sequence, and the outputs of the two directions are spliced together to obtain the final outputs as shown in Figure 3, and which can be described as shown in Equations (18)–(20).

$$\vec{h}_t = \mathrm{LSTM}(x_t, h_{t-1}) \tag{18}$$

$$\overleftarrow{h}_t = \text{LSTM}(x_t, h_{t+1}) \tag{19}$$

$$y_t = W_{\overrightarrow{hy}} \overrightarrow{h}_t + W_{\overleftarrow{hy}} \overleftarrow{h}_t + b_y \tag{20}$$

$\overrightarrow{h}_t$ and $\overleftarrow{h}_t$ represent forward and backward hidden states, and $W_{\overrightarrow{hy}}$ and $W_{\overleftarrow{hy}}$ represent forward and forward weights.

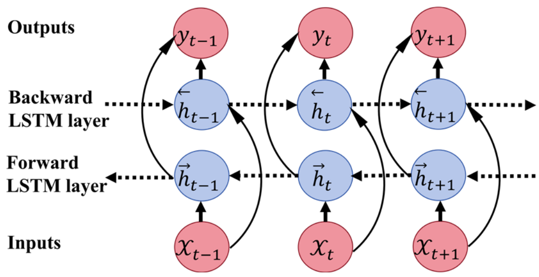

Figure 3. Bipartite process.

The structure of the fault diagnosis neural network used in this paper is shown in Figure 4.

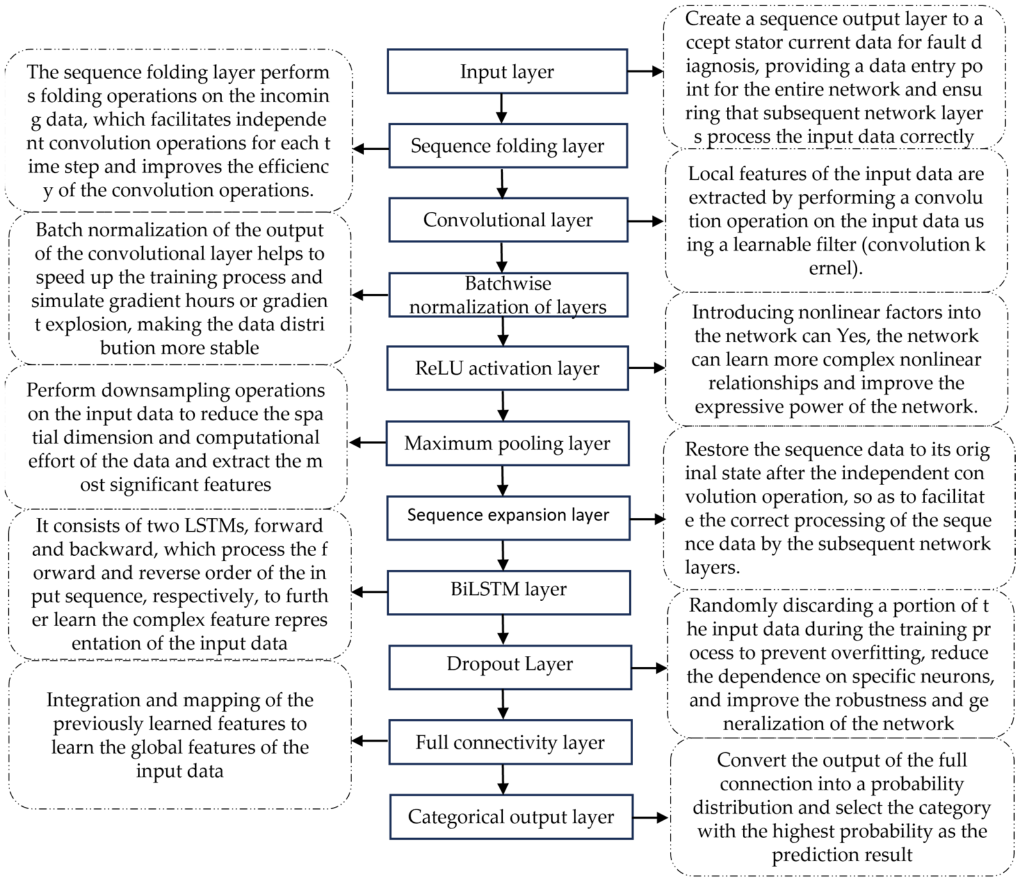

Figure 4. Diagnostic network structure.

CNN-BiLSTM combines all the advantages of CNN and BiLSTM, and compared with CNN and BiLSTM alone, it can extract deeper fault features. Compared with CNN-LSTM, it can better consider the past and future information, so as to more comprehensively extract the temporal features before and after the fault, integrate spatial and temporal dimensions, and make a more accurate fault diagnosis. It has stronger learning ability and robustness.

4. Simulation Experiment Verification

In order to verify the effectiveness of this method for the diagnosis of PMSM turn-to-turn short-circuit faults and demagnetization faults, an eight-pole, twelve-slot PMSM simulation model is established as shown in Figure 5, and the current data of the stator winding are sampled at a frequency of 100,000 times per second, with 12-turn windings in each phase, and the parameters of the motors are set as shown in Table 1 for the normal motors, the turn-to-turn short-circuit faulty motors, and the demagnetization of faulty motors, respectively. The numbering of different health states is shown in Table 2.

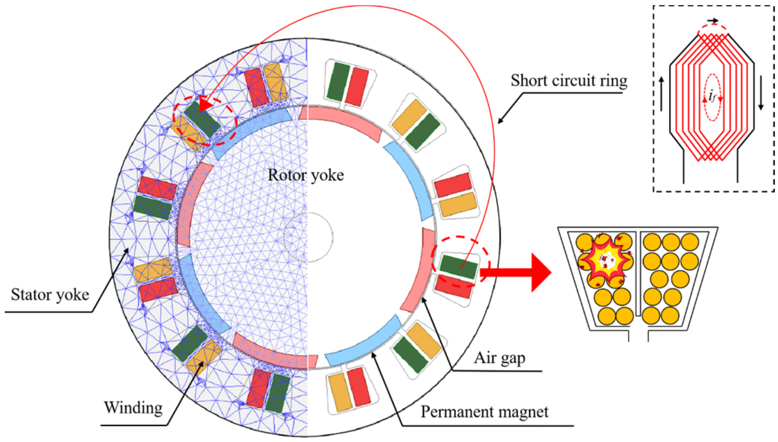

Figure 5. Simulation model of permanent magnet synchronous motor.

Table 1. PMSM parameters.

Parameters	Value	Parameters	Value
Rated power (W)	800	Outer diameter of stator (mm)	120
Peak Voltages (V)	60	Inner diameter of stator (mm)	80
Rated speed (rpm)	3000	Core length (mm)	40
Rated torque (N.m)	15	Outer diameter of rotor (mm)	79
Polar logarithm	4	Inner diameter of rotor (mm)	14.7
Number of grooves	24	Permanent Magnet Type	N38H

Table 2. Status number.

Motor status	Degree of failure	Number
Normal motor	/	D1
Uniform demagnetization	10% uniform demagnetization	D2
	20% uniform demagnetization	D3
	30% uniform demagnetization	D4
	40% uniform demagnetization	D5
Turn-to-turn short circuit	8.33% turn-to-turn short circuit	D6
	16.66% turn-to-turn short circuit	D7
	25% turn-to-turn short circuit	D8
	33.33% turn-to-turn short circuit	D9

Set up the fully healthy state at speeds of 2800 rpm, 2900 rpm, and 3000 rpm and torque angles of 10°, 15°, and 20° for nine conditions, with each condition number as shown in Table 3, and the uniform demagnetization of 10%, 20%, 30%, and 40% and turn-to-turn short-circuit ratios of 8.33%, 16.66%, 25%, and 33.33% for the nine statuses. Fault data collection is carried out, and the different motor fault numbers for each condition are shown in the table; 200 sets of stator current data are collected for each health state, which are divided into two parts: the training set and test set, of which 150 sets are used to train the fault diagnostic network, and the remaining 50 sets are used to test the fault diagnostic accuracy of the trained fault network. Each set of samples consists of 2000 data points, as shown in Figure 6, which shows the three-phase stator current data for different faults at a speed of 3000 rpm and a torque angle of 10°. From the analysis of the figure, it can be seen that both the turn-to-turn short-circuit and demagnetization faults have a significant effect on the magnitude of the stator current, and the uniform demagnetization makes the three-phase stator currents increase in all three phases. The turn-to-turn short-circuit faults have the greatest effect on the stator currents of the faulted phase and also have a certain effect on the other two phases. The stator currents are affected by the turn-to-turn short-circuit faults in the other two phases. In order to improve the robustness and generalization ability of the diagnostic network model and simulate the real environment, adding 30 db noise to all the data, as shown in the figure, produces the modal decomposition of the A-phase current after the addition of noise at a speed of 3000 rpm and a torque angle of 10°, as well as the frequency domain as shown in Figures 7 and 8.

Table 3. Different working conditions.

Velocity/rpm	Torque Angle/°	Number
2800	10 15 20	Z1 Z2 Z3
2900	10 15 20	Z4 Z5 Z6
3000	10 15 20	Z7 Z8 Z9

In order to eliminate the noise in the stator current signal, the signal is decomposed by variational modal decomposition, and then the appropriate modes are selected for data reconstruction to complete the data noise reduction process. In order to obtain the appropriate modal components and need to optimize the number of decomposition layers and the penalty factor, this paper uses the Gray Wolf optimization algorithm to optimize the number of decomposition layers and the penalty factor. When a motor failure occurs, it will cause the arrangement pattern of the current waveform to be more disordered, the arrangement entropy can capture this complexity change well and the calculation process is simple, the minimum value of which can be used as the fitness function to improve the efficiency of the gray wolf algorithm to find the optimal solution. The optimization is stopped when the maximum number of iterations is satisfied, and the optimal number of decomposition layers and the penalty factor are output and substituted into the variational modal decomposition for noise reduction of the original stator current signal.

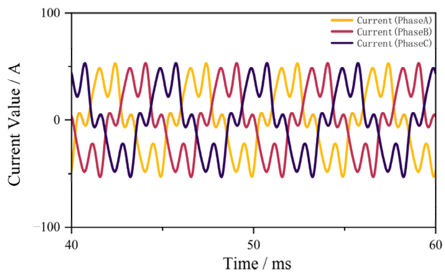

(**a**) normal state

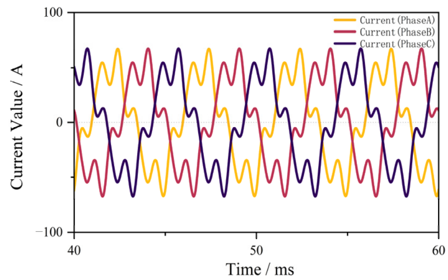

(**b**) 10% uniform demagnetization

Figure 6. *Cont.*

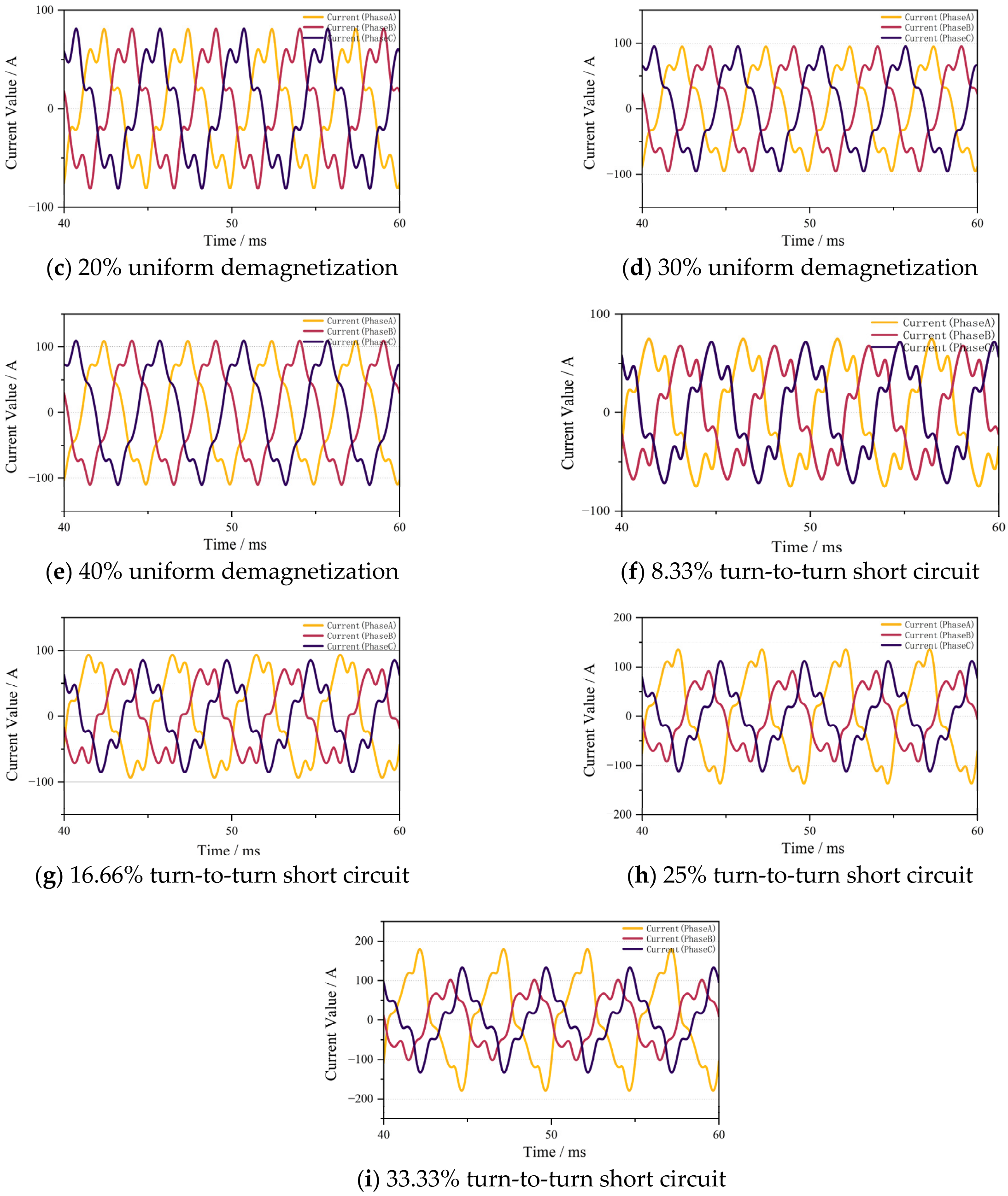

Figure 6. Three-phase stator winding currents under different faults.

The noise reduction processed data are used as the input of the diagnostic network model for network training and testing in order to verify the effectiveness of this paper's use of the Gray Wolf algorithm to optimize the variational modal decomposition parameters for fault diagnosis. It is compared with the CNN-BiLSTM without preprocessing in order to further validate the effectiveness of the proposed method. We propose in this paper's method along with Residual Convolutional Neural Networks (ResCNN) the Multi-scale Convolutional Neural Networks (MsCNN) and other methods for comparison. One of the residual blocks in ResCNN consists of multiple convolutions and is the core part of ResCNN. A residual block contains two paths: one is the regular convolutional layer path and the other is a jump connection that passes the input signal directly to the output, avoiding the attenuation of the gradient when it passes through multiple convolutional layers and making it easier to learn the constant mapping. The core of MsCNN is that it contains multiple convolutional kernels of different scales. In a traditional CNN, a fixed-size convolutional kernel is usually used to extract features, whereas MsCNN uses different sizes of convolutional kernels such as small, medium, and large at the same time. In data processing, a small convolutional kernel may be good at capturing details and local features in the data; a large convolutional kernel is capable of acquiring more macroscopic structural features as shown in Figure 9 for the same working conditions. Fault diagnosis results in a confusing map in different working conditions. Diagnostic results are shown in Figure 10. From the diagnostic results, it can be learned that the method used in this paper has a certain improvement in diagnostic accuracy compared to CNN-BiLSTM without data preprocessing, thus verifying that the preprocessed data in this paper are conducive to the subsequent fault diagnosis, and the comparison between CNN-BiLSTM and ResCNN and MsCNN can also be learned from the method's superiority in diagnostic accuracy. The overall analysis reveals that the method proposed in this paper has improved the fault diagnosis accuracy of PMSM.

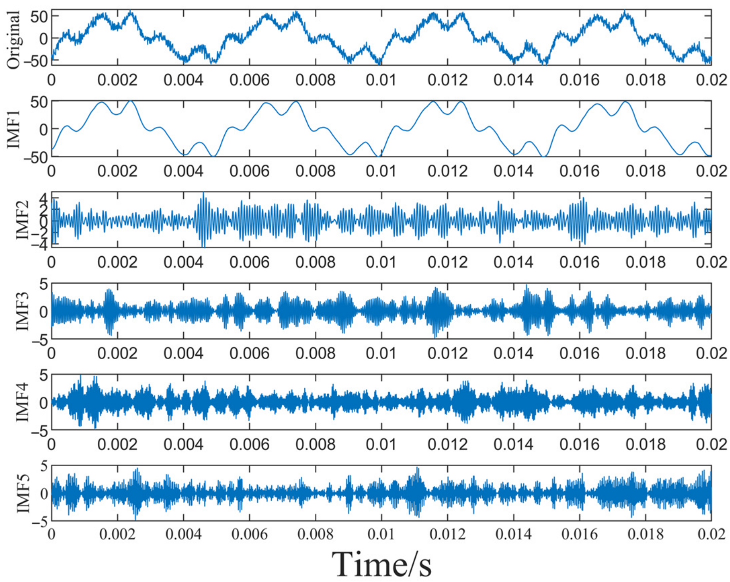

Figure 7. Modal decomposition.

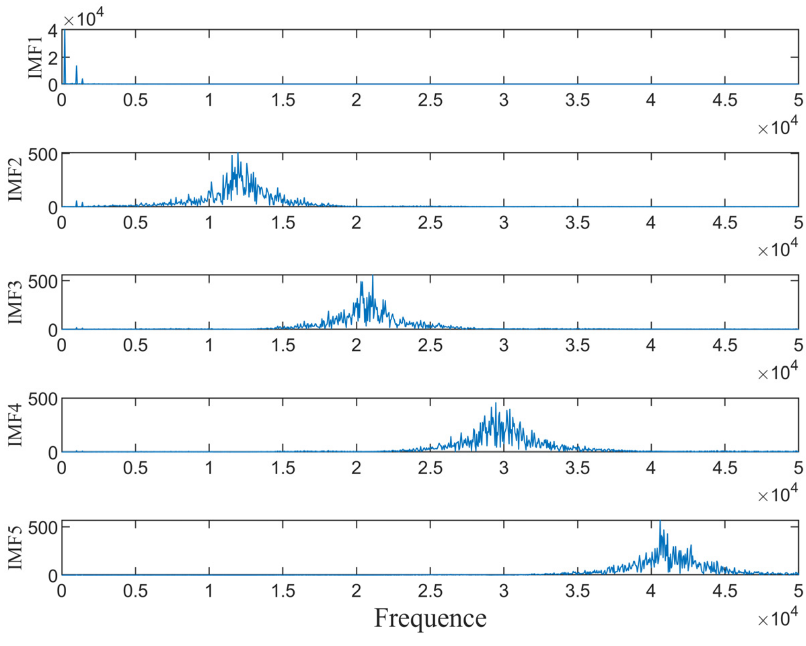

Figure 8. Frequency domain analysis.

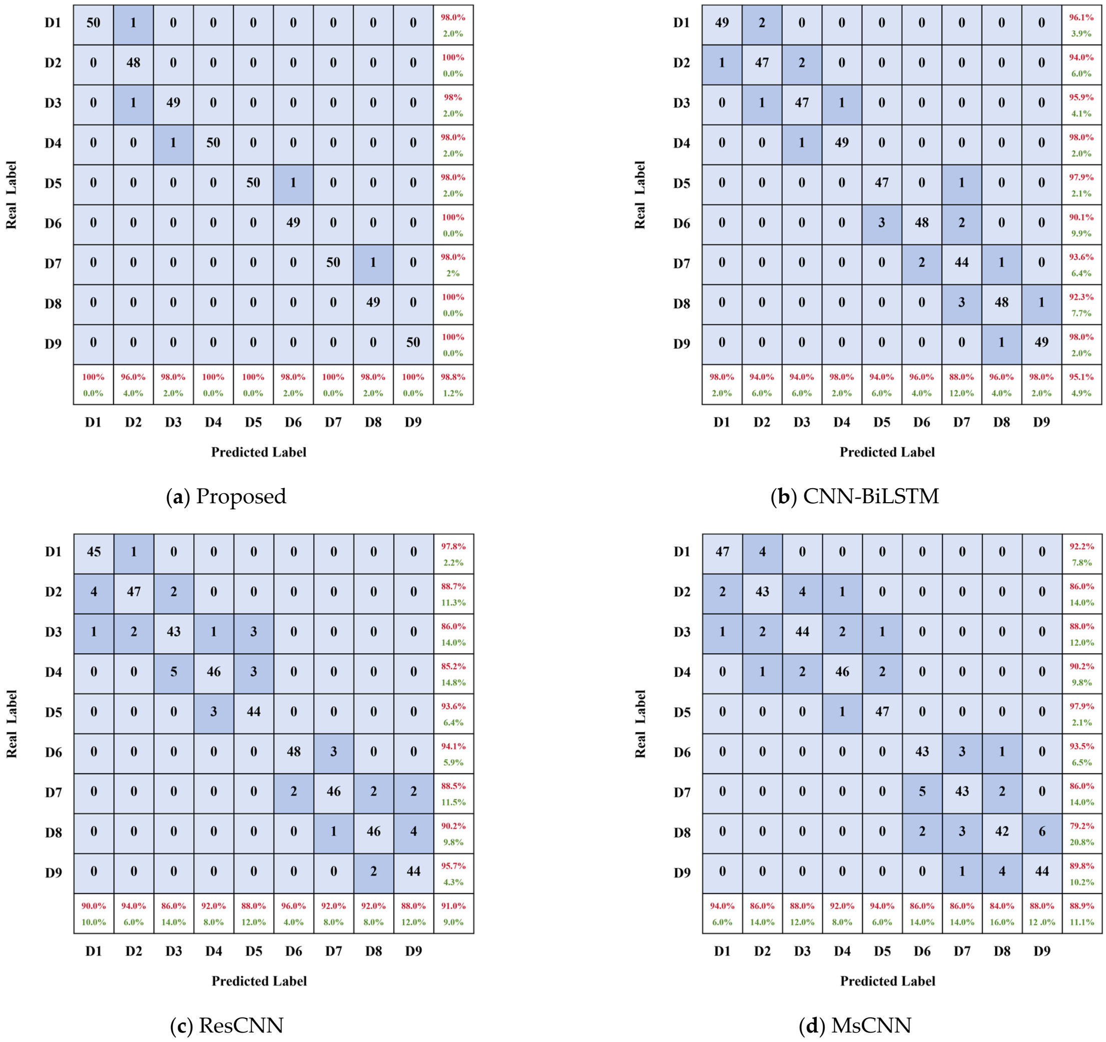

Figure 9. Diagnostic confusion.

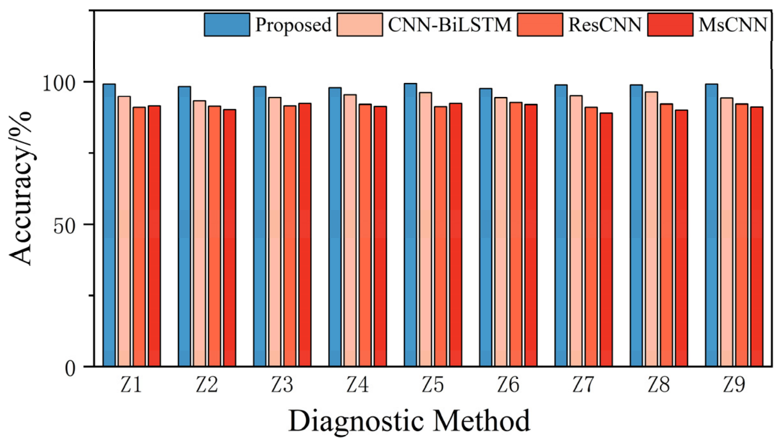

Figure 10. Comparison of diagnostic accuracy under different working conditions.

5. Conclusions

To accurately diagnose the PMSM turn-to-turn short circuit and demagnetization faults, it is proposed to use the Gray Wolf optimization algorithm to optimize the parameters in the variational modal decomposition, to perform noise reduction on the fault signals with noise, and to use the CNN-BiLSTM to diagnose and classify the pre-processed fault signals to realize the fault diagnosis. The simulation results show that this method has certain advantages in the diagnostic accuracy of turn-to-turn short-circuit and demagnetization faults, and the following conclusions are obtained

(1) This paper analyzes the inter-turn short circuit and demagnetization faults of the permanent magnet synchronous motor and shows that with the deepening of the degree of these two kinds of faults, the influence of the stator winding current will be more serious. So this paper chooses the stator winding current as the input signal for fault diagnosis.

(2) The working environment of the permanent magnet synchronous motor is very complex, and the collected fault signals are easily interfered with by noise, so the optimized VMD is used to reduce the noise of the data to reduce the impact of noise on the results of the fault diagnosis, and the optimized VMD is compared with the traditional VMD to achieve automated selection of the parameters, which provides a good condition of the data for the subsequent diagnosis of the fault.

(3) In terms of diagnostic algorithms, the CNN-BiLSTM used in this paper has a certain advantage in diagnostic accuracy compared to other algorithms, and the diagnostic method used in this paper has a certain enhancement effect on the diagnosis of PMSM faults in a comprehensive analysis.

6. Future Work

At present, the method needs to be improved in terms of algorithmic improvement, and a more reasonable network structure can be studied to improve the diagnostic accuracy as well as the general applicability of the method. A complete fault diagnosis system including the data acquisition module, data preprocessing module, model inference module, and result display module can be constructed in future work. Ensuring compatibility and high efficiency between each module, an automated process from motor data acquisition to the output of fault diagnosis results is realized. The model is applied to a real industrial site for validation. In the actual operating environment of a permanent magnet synchronous motor, more complex disturbing factors and changes in working conditions may be encountered. Through a field test, the validity and practicability of the model can be further examined, and the model can be optimized according to the problems in the actual application.

Author Contributions: Y.Y.: methodology-supervision-resources, C.Y.: writing-validation-methodology, D.Z.: supervision-editing-analysis, G.C.: review-analysis, Y.H.: analysis-investigation, J.Y.: analysis-supervision-project management. All authors have read and agreed to the published version of the manuscript.

Funding: This work was supported by the National Natural Science Foundation of China (Grant No. 52067006), the National Natural Science Foundation of China (Grant No. 52462053), the Natural Science Foundation of Jiangxi Province (Grant No. 20232BAB214092; Grant No. 20224BAB214045), the Ganpo Talent Support Program-Leading Academic and Technical Personnel in Major Disciplines of Jiangxi Province (Grant No. 20232BCJ23091), the Key R&D Program of Jiangxi Province (Grant No. 20224BBE51048), the 03 Special Program and 5G Project of Jiangxi Province (Grant No. 20232ABC03A30), and the High-end Foreign Expert Talents Project of the Ministry of Science and Technology of China (Grant No. G2021022002L).

Data Availability Statement: Provision of data will be made on reasonable request.

Conflicts of Interest: All authors declare that they have no conflicts of interest or financial conflicts to disclose.

References

1. Kefalas, T.D.; Kladas, A.G. Thermal Investigation of Permanent-Magnet Synchronous Motor for Aerospace Applications. *IEEE Trans. Ind. Electron.* **2014**, *61*, 4404–4411. [CrossRef]
2. Morimoto, S.; Ooi, S.; Inoue, Y.; Sanada, M. Experimental Evaluation of a Rare-Earth-Free PMASynRM with Ferrite Magnets for Automotive Applications. *IEEE Trans. Ind. Electron.* **2014**, *61*, 5749–5756. [CrossRef]
3. Noguchi, T. Trends of permanent-magnet synchronous machine drives. *IEEJ Trans. Electr. Electron. Eng.* **2007**, *2*, 125–142. [CrossRef]

4. Ozdincer, B.; Aydin, M. Design of Innovative Radial Flux Permanent Magnet Motor Alternatives With Non-Oriented and Grain-Oriented Electrical Steel for Servo Applications. *IEEE Trans. Magn.* **2022**, *58*, 8200304. [CrossRef]
5. Vaez-Zadeh, S.; Ghasemi, A.R. Design optimization of permanent magnet synchronous motors for high torque capability and low magnet volume. *Electr. Power Syst. Res.* **2005**, *74*, 307–313. [CrossRef]
6. Chen, Y.; Liang, S.; Li, W.; Liang, H.; Wang, C. Faults and Diagnosis Methods of Permanent Magnet Synchronous Motors: A Review. *Appl. Sci.* **2019**, *9*, 2116. [CrossRef]
7. Gao, C.; Lv, K.; Si, J.; Feng, H.; Hu, Y. Research on Interturn Short-Circuit Fault Indicators for Direct-Drive Permanent Magnet Synchronous Motor. *IEEE J. Emerg. Sel. Top. Power Electron.* **2022**, *10*, 1902–1914. [CrossRef]
8. Faiz, J.; Nejadi-Koti, H. Demagnetization Fault Indexes in Permanent Magnet Synchronous Motors-An Overview. *IEEE Trans. Magn.* **2016**, *52*, 8201511. [CrossRef]
9. Wu, Y.B.; Zhang, J.Z.; Xu, Z.; Wang, S.S.; Fu, H.J. Feature Extraction and Applicability Comparisons for Fault Detection of Inter-Turn Short-Circuited PMSM. *IEEE Trans. Instrum. Meas.* **2024**, *73*, 3523810. [CrossRef]
10. Yassa, N.; Rachek, M. Modeling and detecting the stator winding inter turn fault of permanent magnet synchronous motors using stator current signature analysis. *Math. Comput. Simul.* **2020**, *167*, 325–339. [CrossRef]
11. Zhou, B.F.; Tang, G.N.; Luo, Y.P. Dynamic Modeling and Analysis of Demagnetizing Rotor of Permanent Magnet Synchronous Motor. *Shock. Vib.* **2021**, *2021*, 6622851. [CrossRef]
12. Liang, H.; Chen, Y.; Liang, S.Y.; Wang, C.D. Fault Detection of Stator Inter-Turn Short-Circuit in PMSM on Stator Current and Vibration Signal. *Appl. Sci.* **2018**, *8*, 1677. [CrossRef]
13. Qi, Y.; Bostanci, E.; Zafarani, M.; Akin, B. Severity Estimation of Interturn Short Circuit Fault for PMSM. *IEEE Trans. Ind. Electron.* **2019**, *66*, 7260–7269. [CrossRef]
14. Song, Q.; Wang, M.S.; Lai, W.X.; Zhao, S.F. Multiscale Kernel-Based Residual CNN for Estimation of Inter-Turn Short Circuit Fault in PMSM. *Sensors* **2022**, *22*, 6870. [CrossRef] [PubMed]
15. Moon, S.; Jeong, H.; Lee, H.; Kim, S.W. Detection and Classification of Demagnetization and Interturn Short Faults of IPMSMs. *IEEE Trans. Ind. Electron.* **2017**, *64*, 9433–9441. [CrossRef]
16. Zhang, Y.; Mao, Y.; Wang, X.Q.; Wang, Z.; Xiao, D.X.; Fang, G.L. Current Prediction-Based Fast Diagnosis of Electrical Faults in PMSM Drives. *IEEE Trans. Transp. Electrif.* **2022**, *8*, 4622–4632. [CrossRef]
17. Hang, J.; Ding, S.; Zhang, J.; Cheng, M.; Chen, W.; Wang, Q. Detection of interturn short-circuit fault for PMSM with simple fault indicator. *IEEE Trans. Energy Convers.* **2016**, *31*, 1697–1699. [CrossRef]
18. Saavedra, H.; Urresty, J.-C.; Riba, J.-R.; Romeral, L. Detection of interturn faults in PMSMs with different winding configurations. *Energy Convers. Manag.* **2014**, *79*, 534–542. [CrossRef]
19. Rosero, J.A.; Romeral, L.; Ortega, J.A.; Rosero, E. Short-circuit detection by means of empirical mode decomposition and Wigner–Ville distribution for PMSM running under dynamic condition. *IEEE Trans. Ind. Electron.* **2009**, *56*, 4534–4547. [CrossRef]
20. Gritli, Y.; Mengoni, M.; Rizzoli, G.; Rossi, C.; Tani, A.; Casadei, D. Rotor magnet demagnetisation diagnosis in asymmetrical six-phase surface-mounted AC PMSM drives. *IEEE Access* **2020**, *14*, 1747–1755. [CrossRef]
21. Fang, J.; Sun, Y.; Wang, Y.; Wei, B.; Hang, J. Improved ZSVC-based fault detection technique for incipient stage inter-turn fault in PMSM. *IET Electr. Power Appl.* **2019**, *13*, 2015–2026. [CrossRef]
22. Hang, J.; Zhang, J.; Xia, M.; Ding, S.; Hua, W. Interturn fault diagnosis for model-predictive-controlled-PMSM based on cost function and wavelet transform. *IEEE Trans. Power Electron.* **2019**, *35*, 6405–6418. [CrossRef]
23. Chen, Z.; Liang, D.; Jia, S.; Yang, L.; Yang, S.; Electronics, S. Incipient interturn short-circuit fault diagnosis of permanent magnet synchronous motors based on the data-driven digital twin model. *IEEE J. Emerg. Sel. Top. Power Electron.* **2023**, *11*, 3514–3524. [CrossRef]
24. Lee, H.; Jeong, H.; Kim, S.; Kim, S.W. Severity Estimation for Interturn Short-Circuit and Demagnetization Faults through Self-Attention Network. *Sensors* **2022**, *22*, 4639. [CrossRef]
25. Al-Greer, M.; Bashir, I.; Demirel, A.; Keysan, O.J.C.; Engineering, E. Autonomous fault detection and diagnosis for permanent magnet synchronous motors using combined variational mode decomposition, the Hilbert-Huang transform, and a convolutional neural network. *Comput. Electr. Eng.* **2023**, *110*, 108894.
26. Ebrahimi, B.M.; Faiz, J. Feature extraction for short-circuit fault detection in permanent-magnet synchronous motors using stator-current monitoring. *IEEE Trans. Power Electron.* **2010**, *25*, 2673–2682. [CrossRef]
27. Huangfu, H.; Zhou, Y.; Zhang, J.; Ma, S.; Fang, Q.; Wang, Y. Research on inter-turn short circuit fault diagnosis of electromechanical actuator based on transfer learning and VGG16. *Electronics* **2022**, *11*, 1232. [CrossRef]
28. Liang, S.; Chen, Y.; Liang, H.; Li, X. Sparse representation and SVM diagnosis method for inter-turn short-circuit fault in PMSM. *Appl. Sci.* **2019**, *9*, 224. [CrossRef]
29. Li, Y.; Wang, Y.; Zhang, Y.; Zhang, J. Diagnosis of inter-turn short circuit of permanent magnet synchronous motor based on deep learning and small fault samples. *Neurocomputing* **2021**, *442*, 348–358. [CrossRef]